# CROSS-VALIDATION OF SINGLE FILAMENT FAILURE BY ACOUSTIC EMISSION AND HIGH-RESOLUTION SYNCHROTRON COMPUTED TOMOGRAPHY

PHILIPP POTSTADA[1], SEBASTIAN ROSINI[2], MARK MAVROGORDATO[2], IAN SINCLAIR[2], S. MARK SPEARING[2], MARKUS G. R. SAUSE[1]
[1]University of Augsburg, Institute for Materials Resource Management, Mechanical Engineering, D-86135 Augsburg, Germany
[2]University of Southampton, Faculty of Engineering and the Environment, Southampton, SO17 1BJ, United Kingdom

**Keywords:** Method combination, Acoustic emission, Synchrotron tomography, Fibre breakage

## Abstract

In this work, we combined acoustic emission measurements and high-resolution synchrotron computed tomography experiments. Samples were prepared as double-edge notched tensile specimens with $[90_2/0_2]_s$ layup. With a voxel size of 0.65 µm, we were able to identify the presence of fibre breakage clusters within a field of view of ~ ± 0.5 mm around the centre of the notches. The number of fibre break signals was directly counted as function of load steps, along with the formation of groups of interacting fibre breaks (clusters). This was compared to the simultaneously acquired acoustic emission signals using two miniature multi-resonant piezoelectric sensors. The signal sources were localized along the length axis of the specimen and only the acoustic emission sources within the field of view were considered for further evaluation. Signal interpretation is presented in terms of failure mechanisms observed directly via synchrotron radiation computed tomography images, and on the basis of established pattern recognition techniques within the acoustic emission. Given the explicit and precise representation of fibre breaks achievable via synchrotron radiation computed tomography, a uniquely detailed correlation between failure processes and acoustic emission events is achieved during loading.

## 1. Introduction

Several experimental approaches exist to investigate *in situ* the evolution of damage in fibre-reinforced polymers. Among them, synchrotron radiation based computed tomography (SRCT) and acoustic emission (AE) analysis proved to be compelling tools to visualize damage formation and evolution, as well as to concisely analyse their dynamics [1–5]. A special emphasis is given in this work to the detection of fibre breaks and their interactions, as these are the load carrying constituents of the composite and hence, their failure acts as initiation of macroscopic failure of the component [6]. However, while SRCT provides a high fidelity in the detection of the break position, the temporal resolution is still limited to the exposure time and number of projections acquired per scan, resulting in scan times commonly in the order of minutes.
AE analysis ensures a synchronous acquisition of the acting load and the AE signals, providing extraordinary temporal resolution of the occurrence of microscopic damage, such as fibre breaks. The rapid internal displacement caused by such fibre breakage is known to cause acoustic emission signals. In previous work, acoustic emission associated with this type of failure were identified by multivariate data analysis [7] with their acoustic signature being validated by finite element modelling [8]. Combined with the possibility to distinguish different failure mechanisms, this allows for a dedicated analysis of the growth of damage. However, the accuracy of source localization is limited based on the distance of the AE sensors and the correct determination of the arrival time. Typically, this can result in a range of a few millimetres at best, which is acceptable for large composite structures, but not sufficient enough for precise localisation of single fibre breaks in smaller specimens.

Thus, the combination of both methods offers a completely new view on the damage formation in composite materials and was explored in this level of detail for the first time in an ongoing collaborative project. A long-term objective of this project is to visualize and understand the formation of the first single fibre breaks and the subsequent occurrence of multiple fibre breaks in close proximity, which ultimately lead to a macroscopic failure of the composite. This paper presents initial data demonstrating capabilities to acquire AE-signals during *in situ* SRCT loading at the European Synchrotron Radiation Facility (ESRF) in Grenoble France. In this paper we demonstrate that the acquired AE signals and visually identified fibre breaks can be correlated in a reasonable manner.

## 2. Experimentation

### 2.1. Equipment

The microtomography beamline ID19 at ESRF was chosen. For the *in situ* acquisition, a combination of a MISTRAS PCI-2 AE-system and a modified DEBEN CT5000 tensile stage was used [1, 9]. The AE measurement chain consists of a miniature multi-resonant sensor HD2WD from MISTRAS. Two AE sensors were used to allow a one-dimensional AE source localization. The acquired signals were amplified by a MISTRAS 2/4/6 pre-amplifier and were subject to a built-in analogue 20-1200 kHz band-pass-filter. Preamplifiers were mounted on the rotation table close to the *in situ* tensile load stage. The amplified AE signal was led outside the experimental hutch using a standard RG58 coaxial cable, which connects to the PCI-2 acquisition card. The acquired signals were recorded with the MISTRAS software AEwin™. Load was applied via the DEBEN CT5000 stage connected via the associated controller box to a standard PC using the Microtest software provided by DEBEN U.K. While the drive unit and the load cell of the tensile stage remained unmodified relative to the commercial setting, the load introduction concept of the specimen was modified (see Figure 1).

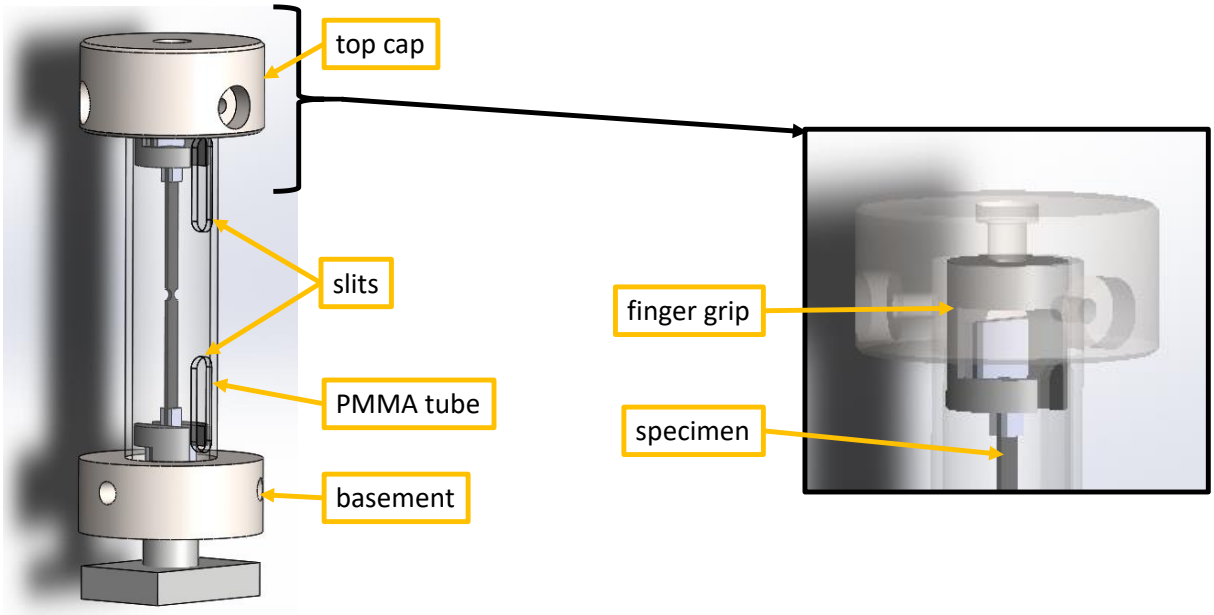


**Figure 1**. Modified part of the in situ tensile stage with finger grip clamping system and PMMA tube with two slits for acoustic emission sensors cables (a). Scans from laboratory µ-CT scanner with artefacts related to the acoustic emission sensor cables passing through the X-ray beam path (b).

The load was introduced via a finger grip system, which ensures a simple assembly of the specimen and a proper load transfer into the specimen after reaching a slight pre-load. The upper finger grip was statically fixed in a top-cap, which transferred the load via a PMMA tube using form closure into a custom-made frame of the tensile stage. To ease assembly of the PMMA tube, it was held in position with three screws.
Prior scans were collected using a laboratory micro-focus X-ray CT scanner, Zeiss 160 kVp Versa 510, at the µ-VIS Imaging Centre at the University of Southampton, evidencing artefacts generated by the AE sensors cable passing through the X-ray path. Considering the necessity of using automated approaches for processing the large amount of data generated during the test campaign, artefacts were avoided by machining two slits on the PMMA tube. This avoided the cables passing through the X-ray path (cf. Figure 2). For synchronous evaluation of mechanical load and acoustic emission data, the controller of the tensile stage and the AE-system were connected. With this, the current force values were fed into the AE system by a proportional analogue voltage signal, which allowed a synchronised acquisition of load and AE-signals.

## 2.2. Specimen preparation

Double edge notched tensile specimens were manufactured via waterjet cutting (as indicated by Wright *et al.* in [10]) from $[90_2/0_2]_{sym}$ carbon/epoxy pre-preg laminate plates produced by Mitsubishi Chemical Co. Specimens were tabbed with adhesively bonded T-shaped aluminium ends. A grinding and cleaning phase on the contact surface between tabs and coupons took place before application of the fast curing methyl-methacrylate adhesive. To ensure adhesion and mechanical stability of the AE sensors on the specimens, holders fabricated out of polylactide by additive manufacturing and rubber rings were used. To obtain a repeatable and correct positioning of the support structure, the holders were provided with four integrated dowel pins (as indicated in Figure 1 and
Figure **2**).

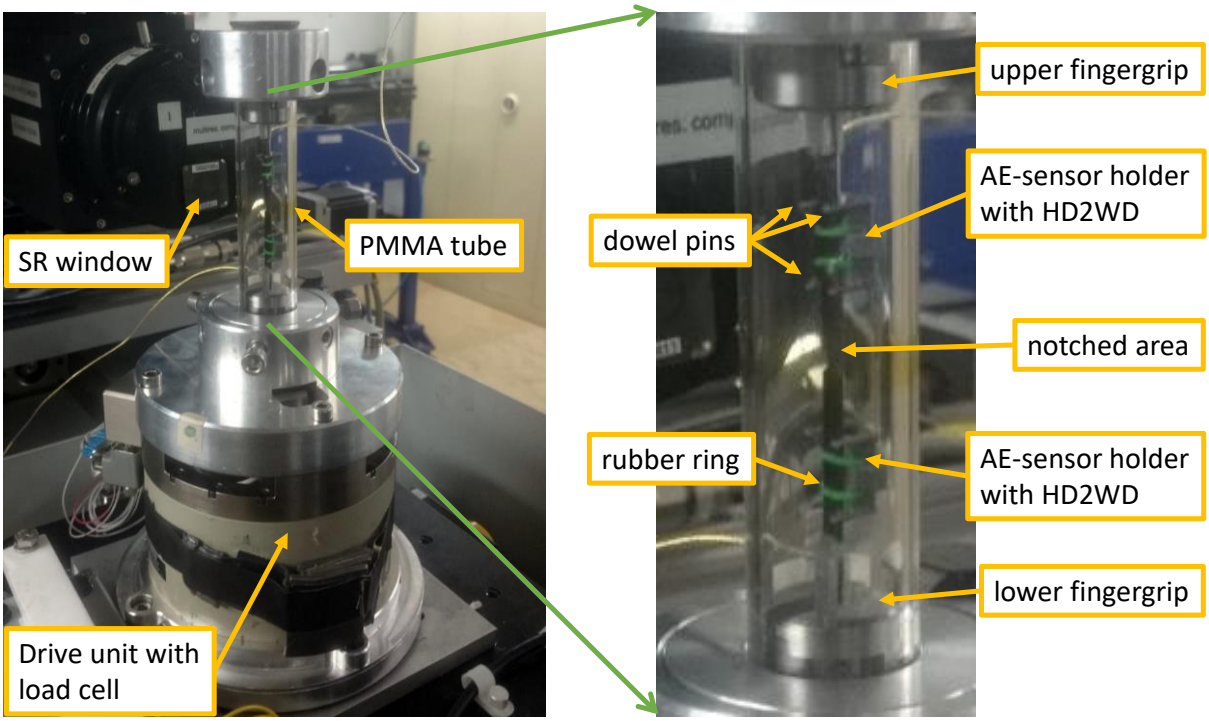


**Figure 2.** *In situ* tensile stage with installed specimen and AE sensors ready for testing

### 2.3. Testing procedure

At the beginning of each test, three pencil lead breaks (PLB) were performed at the base of the tensile stage to ensure a sufficient coupling of the AE-sensors to the specimen. The setting used for the AE-acquisition for both sensors where a threshold of $35dB_{AE}$ at $40dB_{AE}$ pre-amplification and a Peak Definition Time (PDT) of 10µs, a Hit Definition Time (HDT) of 80µs and a Hit Lockout Time (HLT) of 300µs. The AE signals were acquired with a sampling rate of 10 MS/s.
After a satisfactory pre-check the AE-acquisition was started. A first SRCT scan was collected to record the initial (undamaged) specimen volume. To ensure a stable positioning of the specimen in the beam path, a load of 100 N (representing five to seven percentages of the sample ultimate tensile strength (UTS)) was applied. At this load level, no pre-damage was observed. The drive unit was switched off and the cross-head position was kept constant by the self-locking mechanics of the loading stage. The scan was performed continuously with beam energy of 19.5 keV. During each tomographic scan, 2996 projections with an exposure time of 50 ms were collected at a detector distance of 50 mm. The voxel size was 0.65 µm.
After the end of the first scan, the specimen was loaded by a constant displacement rate of 0.2 mm/s to 60 % of the calculated ultimate tensile strength (UTS). During the loading all AE-signals were acquired. Then, a second SRCT-scan was carried out. This procedure was repeated for 80 %-UTS, 90 %-UTS and subsequently in increments of 2 %-UTS until specimen failure.

### 2.4. Processing of AE-data

For the acquired AE signals, a feature extraction was performed. Besides the common AE feature values of amplitude, energy, duration, also the partial powers of six equal frequency ranges of 150 kHz width, ranging from 0 MHz to 1 MHz were calculated out of the first 35 µs after the arrival time. The arrival time was calculated using the Akaike information criterion (AIC) [11]. In addition, spectral feature values, such as the weighted peak frequency were calculated [7]. AE source localization was performed by a classical Δt-based algorithm considering the given geometry of the specimen and the sensor positions. The velocity of sound was measured for each material using time-of-flight tests on the raw material plates before cutting the test geometries. Only the localized AE-signals were used for the following evaluation.
A pattern recognition approach following [7] was performed using a Gustafson-Kessel algorithm allowing a maximum number of P=6 clusters and a minimum number of M=4 features for twelve previously selected list of frequency features K. The selected features are reverberation frequency, average frequency, initiation frequency, partial power 1-6, peak frequency, frequency centroid and weighted peak frequency. The resulting clusters from this optimization procedure are shown in Figure 3-a and allow the separation of AE-signals based on their frequency characteristics. Based on earlier studies, these can be attributed to the occurrence of matrix-dominated failure and fibre dominated failure modes [7, 8]. The corresponding AE source position (x-position) along the specimen axis is shown superimposed to the load-hold cycles in Figure 3-b. While most of the damage occurs close to the notch position, still numerous AE sources are also active outside this region. With increasing load steps, the AE source density indicates a growth of damage from the notch position outwards. Members of both clusters are found distributed along the length axis of the specimen.

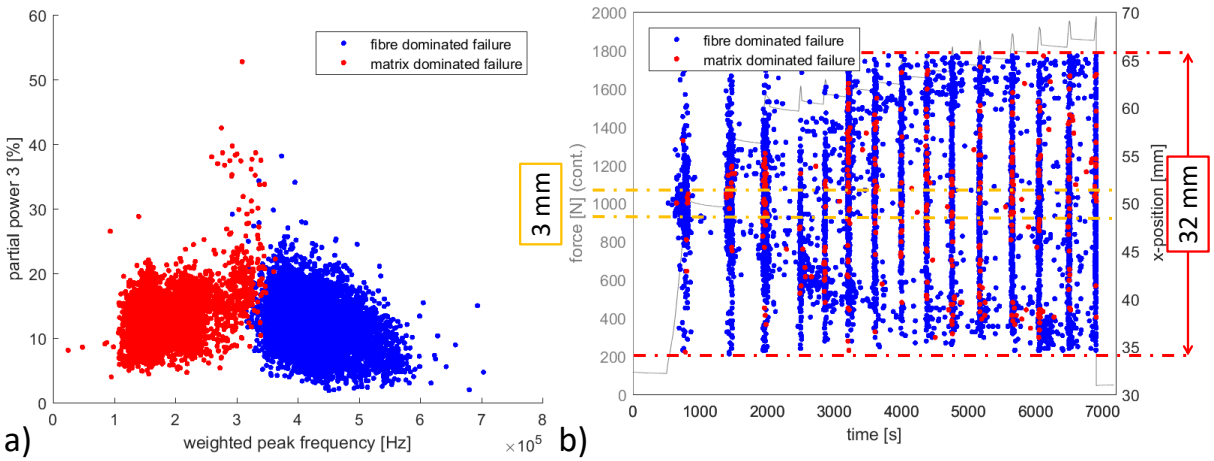


**Figure 3**. Visualization of clustering result using the partial power between 300-450 kHz and weighted peak frequency (a). The blue cluster at higher frequencies represents fibre-dominated failures whereas the red cluster at lower frequencies represents matrix-dominated failure. Applied load-hold cycles and localized AE-signals as function of time (b)

## 2.5. Processing of the SRCT data: automated fibre segmentation method

An automated approach has been adopted to process the data generated during the synchrotron test campaign. In Figure 4, the specimen geometry with the imaged volume are represented, together with one of the slices from which fibre breaks are segmented. In Figure 4-c, an example of the top view of the fibres as obtained after reconstruction of the data, with a single fibre break and two closely co-planar adjacent breaks forming a fibre break cluster are shown.

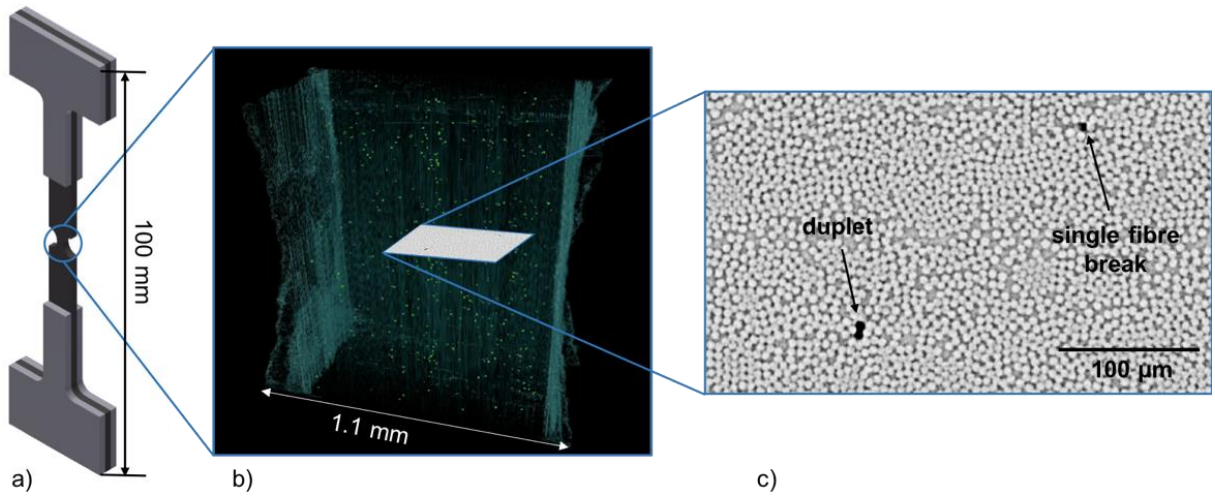


**Figure 4.** a) Sample geometry with approximate region of interest of all the scans b) 3D segmentation of the fibre breaks within the bulk material c) top view of the 0 degree layers with a single fibre break and two closely co-planar adjacent breaks forming a fibre break cluster.

Each processed volume consisted of approximately 2000 slices, which were assessed with an automated approach for fibre break detection. Using a macro written in ImageJ™, the volumes collected from low to high strains are loaded and converted from 32-bit to 8-bit to reduce the file dimensions without losing fidelity in the feature representation. The user is asked for manual input to select the region of interest,

which is kept the same for all the scans. The data is then passed to MATLAB™ (but same image processing procedures can be achieved in ImageJ™, for which the reader can find a complete guide in [9]). Image quality is improved by contrast adjustments, followed by a median filter to remove noise but preserve sharp edges of the fibre breaks. An appropriate threshold value chosen *a priori* by visual inspection is adopted for the break segmentation in all the scans. As the distance between crack faces of a fibre break has been observed to extend for between 2 and 4 µm (i.e. considered a voxel size of 0.65 µm, for about five slices), one break shown in different consecutive slices is then connected in 3D using the algorithms 'bwconncomp' and 'regionprops', in MATLAB™ version 2017b. These respectively look for close unlabelled pixel of the same intensity until all pixels are labelled and provide properties of the 3D detected feature (e.g. coordinates of the centre of mass and volume) [12].

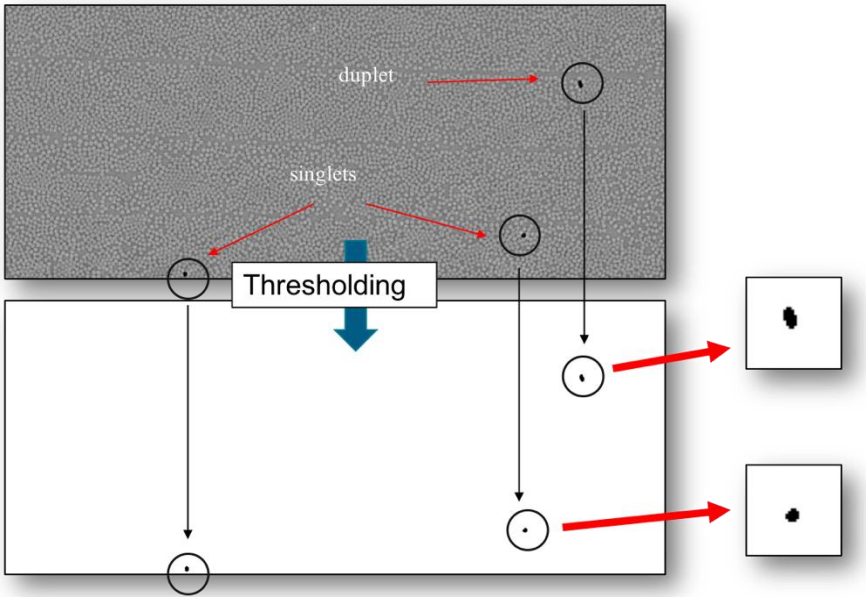


**Figure 5.** Segmentation approach for the breaks accumulation evaluation. Scripts have been developed, using appropriate threshold values. From the binary image, 3D connected components (representing the fibre breaks) are recorded and labelled.

## 3. Results

Considering the present data sets, we correlate the absolute number of fibre breaks identified by AE-signals and by SRCT count. In Figure 6, there is a common growing trend for the load range beyond 90% ultimate tensile strength. Taking into account all AE signals identified as fibre breakage, the absolute number shows an obvious mismatch to the SRCT data. Based on the Δt-based source localization algorithm, these AE signals originate from the x-distance of 32 mm around the notch position. Accordingly, there is a huge mismatch to the inspection range of SRCT (x-distance of ~1 mm around notch position). Therefore, we removed all fibre breakage AE signals outside the notch area (x-distance ~3 mm) based on filtering of their source location (cf. Figure 3-b). Their numbers are reasonably close to the SRCT fibre breakage counts and both trends correlate well. Based the expected accuracy of the AE source localization is in the order of some millimetres, we assume the 3 mm distance to be an appropriate choice. Further reduction of distance (e.g. to 1 mm) would systematically lower the number of signals, but there is large likelihood, that because of localization errors, a significant portion of fibre breakage signals are outside this range, although they fall well within the SRCT observation range. This is also confirmed by similar results, which were obtained for the other specimens investigated.

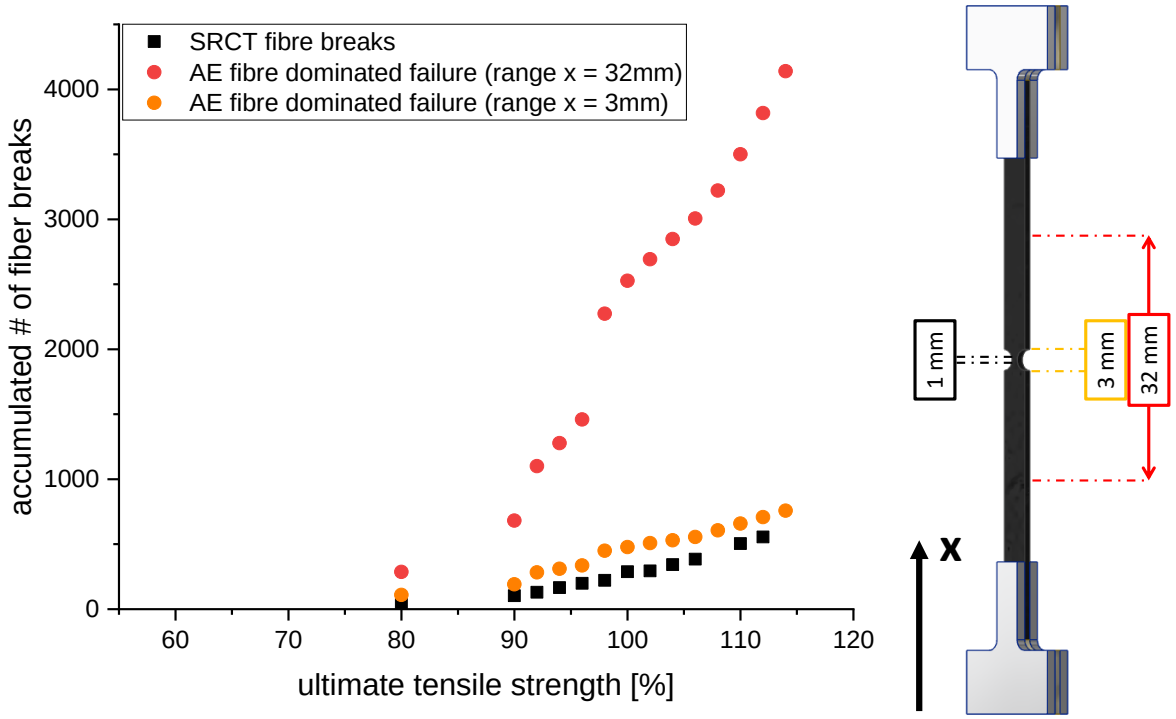


**Figure 6.** Recorded counts for fibre breaks detected by SRCT and fibre dominated failure AE with respect to different x-distance evaluation ranges for one representative specimen with first load step at 80 %-UTS

## 4. Conclusions

In this work, we presented a modified setup for *in situ* tensile SRCT testing with combined AE-acquisition. The proof of concept for this combination is delivered by a test campaign at the beamline ID 19 at the ESRF. In a first attempt, the recorded AE-signals were divided in two clusters, representing matrix and fibre dominated failure modes. The amount of fibre breakage AE-signals localized in the notch area compared well with the SRCT fibre breakage count. The remaining mismatch of the absolute numbers is partially credited to the different evaluation volumes and should be statistically confirmed within ongoing experiments on this topic.
After cross-validation of both methods (SRCT and AE), a huge potential exists to reveal the dynamics of fibre breakage accumulation and local agglomeration of multiple fibre breaks, that ultimately results in laminate failure.

## Acknowledgments

The authors would like to acknowledge the European Synchrotron Radiation Facility for provision of synchrotron radiation facilities and would like to thank Dr Lukas Helfen and Ms Elodie Boller for assistance in using beamline ID19. The authors also gratefully acknowledge Mitsubishi Chemical Co. for materials supply and the µ-VIS X-Ray Imaging Centre at the University of Southampton for provision of tomographic imaging facilities, supported by EPSRC grant EP-H01506X.

## References

[1] S.C. Garcea, I. Sinclair, S.M. Spearing. Fibre failure assessment in carbon fibre reinforced polymers under fatigue loading by synchrotron X-ray computed tomography. *Composites Science and Technology*, 133: 157–64, 2016.
[2] A.E. Scott, M. Mavrogordato, P. Wright, I. Sinclair, S.M. Spearing. In situ fibre fracture measurement in carbon–epoxy laminates using high resolution computed tomography. *Composites Science and Technology* 12, 71: 1471–7, 2011.
[3] Y. Swolfs, H. Morton, A.E. Scott, L. Gorbatikh, P.A.S. Reed, I. Sinclair, S.M. Spearing, I. Verpoest. Synchrotron radiation computed tomography for experimental validation of a tensile strength model for unidirectional fibre-reinforced composites. *Composites Part A: Applied Science and Manufacturing*, 77: 106–13, 2015.
[4] Hamstad M.A. Thirty years of advances and some remaining challenges in the application of acoustic emission to composite materials, 2000.
[5] G.A. Ono K. Research and Applications of AE on Advanced Composites, 2012.
[6] S. Blassiau, A.R. Bunsell, A. Thionnet. Damage accumulation processes and life prediction in unidirectional composites. *Proceedings of the Royal Society A: Mathematical, Physical and Engineering Sciences* 2080, 463: 1135–52, 2007.
[7] M.G.R. Sause, A. Gribov, A.R. Unwin, S. Horn. Pattern recognition approach to identify natural clusters of acoustic emission signals. *Pattern Recognition Letters* 1, 33: 17–23, 2012.
[8] M.G.R. Sause, S. Richler. Finite Element Modelling of Cracks as Acoustic Emission Sources. *J Nondestruct Eval* 1, 34: 264, 2015.
[9] S.C. Garcea, M.N. Mavrogordato, A.E. Scott, I. Sinclair, S.M. Spearing. Fatigue micromechanism characterisation in carbon fibre reinforced polymers using synchrotron radiation computed tomography. *Composites Science and Technology*, 99: 23–30, 2014.
[10] P. Wright, A. Moffat, I. Sinclair, S.M. Spearing. High resolution tomographic imaging and modelling of notch tip damage in a laminated composite. *Composites Science and Technology* 10, 70: 1444–52, 2010.
[11] Akaike H. Markovian representation of stochastic process and its application to the analysis of autoregressive moving average processes. *Ann. Inst. Stat. Math.* 26: 363–87, 1974.
[12] MathWorks. Image Processing Toolbox TM. *User ’s Guide*.